EUROPEAN COOPERATION
IN THE FIELD OF SCIENTIFIC
AND TECHNICAL RESEARCH

EURO-COST

COST 2100 TD(XX)XXX
Aalborg, Denmark
June 02-04, 2010

SOURCE: - TREL, Toshiba Research Europe Limited
- University of Bristol
United Kingdom

# Ultrawideband Pulse Correlation and Distance Error Estimation

Rafael Cepeda[1], Mark A. Beach[2] and Joe P. McGeehan[1,2]
[1] *Toshiba TRL*
32 Queen Square
Bristol, BS1 4ND
UNITED KINGDOM
[2] *University of Bristol*
Department of Electrical and Electronic Engineering
Merchant Venturers Building, Woodland Road
Bristol, BS8 1UB
UNITED KINGDOM
Phone: + 44 (0) 117 906 0700[1]
Fax: + 44 (0) 117 906 0701[1]
Email: {Rafael, Joe}@toshiba-trel.com,
M.A.Beach@bris.ac.uk

# Ultrawideband Pulse Correlation and Distance Error Estimation

Rafael Cepeda, Mark A. Beach and Joe P. McGeehan

**Abstract**

In a given number of wireless systems, and ultrawideband (UWB) in particular, a way to communicate between transceivers is by correlating received pulses with one or several reference-pulse templates. The reference template(s) aim to give a good representation of the transmitted signal. However, even for unscattered signals, resulting from line-of-sight (LOS) transmissions, radiated pulses may differ as a function of the antennas' angle of departure/capture or may "look different" due to limited spatial resolution at the receiver. As these inaccuracies are often neglected and may have an impact on the robustness of a communication's link, unscattered LOS UWB measurements, from 3.5 GHz to 10.5 GHz, are used in this paper to explore: (i) the effects of correlating received signals with different pulse templates as a result of distance changes between antennas (shorter than the spatial resolution of the system) and different angles of antenna radiation/capture; and (ii) the error in distance prediction from a system relaying on peak detection and limited by its spatial resolution. As a result, pulse correlation values were found to fluctuate from one and up to a value of 0.4 in some cases. Also, errors in distance estimation were characterised against different interpolation factors, from which modelling parameters are presented.

## 1 Introduction

Pulse correlation is currently used in different systems to determine the presence of a desired signal or terminal location [1–3]. Signals are detected, but sometimes it is required to have a better interpretation of them to achieve a clearer, or more accurate, estimation of travelled distance or their distortion. The accuracy is partially determined by the fidelity of the received pulse and its correlation with a previously stored template [4]. In the case of a sounding system, accuracy in wireless propagation channel estimation is bounded by physical and systematic constraints. Some of these constraints are determined by: precision of equipment (i.e. timing, calibration, temperature stability, interference); the test signal (range resolution); and the antenna gain and pattern alignment. Nevertheless, the use of "perfect" signals is widely accepted for characterising measurements or do simulations.

For instance, the effects of noise on pulse cross-correlation has been investigated for Sonar applications in [5] assuming perfect alignment of signals. Regarding ultrawideband (UWB) systems, [6] also considered perfect pulse alignment for the simulation of accurate location systems.

Moving into more realistic scenarios, additional differences in the received signals are produced when the radiated signals have departed and are received at different elevation and/or azimuthal angles. This characteristic of the antennas in the transceivers makes the radiated UWB pulses to exhibit *different shapes*, which is a problem that happens even for unscattered signals. Consequences of this problem have been partially investigated for two different UWB antennas, where a pulse from a fixed transmit angle was correlated with different angular templates [7].

Regarding the propagation of signals and the impact of correlation, researchers in [8] analyse the interaction of UWB signals and the environment, and present a statistical analysis of UWB channel

correlation functions. Also, the use of multiple pulse-templates was considered in [9] to deconvolve the antenna response from channel impulse responses (CIRs), in the time domain, by using the *CLEAN algorithm*[1], originally introduced by Högbom in 1974 for a single pulse template [10][2].

Since the sampling resolution of UWB channel sounders is limited, the received pulses, which last for several sampling points, have different shapes as a result of signals being captured and sampled with different associated delays. Hence, it is very likely that some pulses in a line-of-sight (LOS) CIR will not be captured in such a way that a sample is taken at the exact location of its peak value. In consequence, if the distance between transmit and receive antennas, or the time of arrival of each delayed signal, is calculated from the sampling with strongest power, certain level of uncertainty is produced. Yet, characterisation of the propagation channel has been done by using only one pulse template in the time domain to achieve better resolution, i.e. [11].

Pulse distortion is an important issue in UWB measurements since several multipath components may be received, and discriminated, after being affected by the frequency-dependent scattering environment [12]. These signals arrive at the receive antenna after travelling throughout the propagation channel, which, in turn, produces different delays that are not necessarily aligned in time with the sampling period of the sounder. Therefore, if only one pulse template is employed to find these pulses, an inaccurate representation of the propagation channel may result.

So far, changes on pulse templates as a result of limited spatial resolution in measuring equipment have not been considered. In addition, as not an infinite number of pulse templates can be used for deconvolving the antenna response from measurements, it is important to know if received pulses, with infinitely many delays, can be derived from the fast Fourier Transform (FFT) interpolation, [13], of any measured pulse template and then used as source for dynamic pulse template generation. In turn, these pulses could be used to create an adaptive input parameter to the, for instance, CLEAN algorithm.

The pulse correlation distortion due to sampling limitation and angle of radiation, and the error in distance estimation are studied in this work. To this end, sets of CIRs were captured and analysed from two experiments conducted in a modern open-plan office environment and an anechoic chamber. The environments were enquired by using a time domain channel sounder, which performs a periodic sub-sampling of the spectrum of interest. Both experiments consist of unscattered LOS single-input single-output (SISO) measurements.

The first experiment initially aims to characterise the pulse correlation fluctuations in two circumstances: when the distance between transmit and receive antennas varies in a smaller proportion than the sampling period of the sounding equipment; and when the azimuthal angle of radiation varies. The second aim of this experiment is to show that interpolated pulses, using the FFT interpolation method, measured at different distances between transmit and receive antennas produce very similar pulse templates. This, however, leads to the conclusion that using a single pulse template to retrieve the energy from a measured CIR may conduct to misleading results. Based on results from these tests, in the second experiment, an FFT interpolated pulse is used to calculate the error in distance estimation between transmit and receive antennas, at different locations, in a bi-dimensional grid of points.

After having defined our ground of work (above), the rest of the paper is organised as follows: First, the sounding equipment is introduced in Section 2 and the practical experiments described in Section 3. The analytical method and results are presented next in Section 4 and, finally, conclusions are given in Section 5.

[1]The algorithm assumes that the CIRs are the result of a number of point sources. CLEAN iteratively finds the CIR's maximum and subtracts a weighted version of this point source convolved with a point spread function (dirty map) of the observation. This is done until the CIR's maximum is smaller than a given threshold.

[2]Initially derived to deconvolve images in radio astronomy.

## 2 Sounding Equipment

We use a periodic sub-sampling (PS) time-domain sounder [14] and biconical antennas [15, 16] to interrogate the ultrawideband (UWB) channel in the 3.5 to 10.5 GHz band.

Fig. 1 shows the configuration of our sounding equipment. A "master controller" laptop computer remotely drives the servo-positioning system (turntable and/or $x, y$ positioners [17]) via RS232/USB and the PS sounder via TCP/IP. This computer also monitors the sounded environment using a USB video link. At a convenient distant location, a "remote controller" laptop computer provides the interface to operate a spectrum analyser (SA) and the whole sounding process by accessing the master controller via TCP/IP. We use this additional computer to centralise the control of the experiments and to avoid any unwanted movement or human intervention in the sounded location. The SA (Agilent PSA E4440A) is connected to a biconical antenna through an Agilent 83006A low-noise amplifier (LNA) to detect interferers and to continuously check the "health" of the test signal.

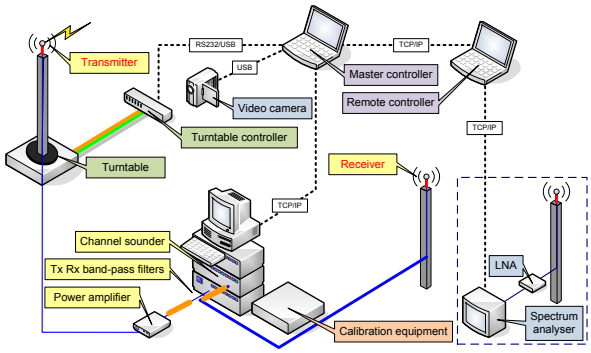


**Figure 1:** Diagram of the UWB sounding system layout.

The PS sounder, manufactured by MEDAV and internally depicted in Fig. 2, has two sequential transmitters and four parallel receivers. Thus, being able to enquire $(2 \times 4)$ multiple-input multiple-output (MIMO) complex wireless propagation channels by using trains of pseudo-noise (PN) sequences, or $m$-sequences. Each of the sequences consist of 4,095 pulses, or chips, generated in baseband by a linear feedback $n$-stage shift register at a clock rate of $f_c = 6.947$ GHz. The test signals are later up-converted, using the same clock, to cover the bandwidth from 3.48 to 10.43 GHz. Based on these parameters, the PS sounder has a delay resolution of 143.9 ps or a spatial resolution of $s_r = 4.31$ cm.

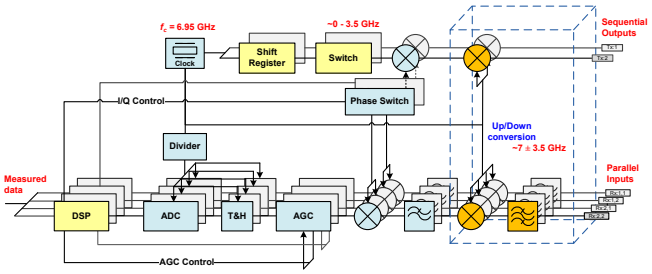


**Figure 2:** Architecture of the $(2 \times 4)$ periodic sub-sampling UWB MIMO sounder.

Once the test signals have been generated by the PS sounder, they are band-pass filtered to avoid out-of-band emissions, amplified (Agilent 83020A), transferred to biconical antennas for radiation

and, after travelling through the propagation environment, received by similar antennas connected to band-pass filters. In turn, the receiver down-converts captured signals and corrects their gain by using an automatic gain control (AGC) unit, with 33 dB dynamic range in steps of 3 dB. The AGC prevents the system from saturation and amplifies weak received signals to a certain degree. The received signals are then periodically sub-sampled and a phase shifter is used to allow the sampling of complex channel impulse responses (CIRs) in the time domain. The analogue signals are subsequently digitalised, using an analogue-to-digital converter (ADC) and, finally, a matched filter, using the known PN sequence, is implemented and used in a digital signal processing (DSP) unit.

Depending on configuration, a certain number of CIRs is internally averaged and the result transferred to a digital storage unit as final-user data. The averaging process mitigates the effects of noise in the measurements and provides a more relaxed data-transfer rate.

Before sounding and after an equipment's warming-up period of approximately one hour, the system response, phase imbalance and crosstalk are characterised using cabled or open-loop connections. The measured parameters are then used for calibration to only leave the combined response of the antennas and the environment on the data recordings.

The periodicity of the transmitted $m$-sequences has both advantages and disadvantages. Firstly, it allows the sampling of signals at a more relaxed rate without significant degradation. This makes possible the construction of reduced complexity receivers. Secondly, a *range ambiguity* or range folding effect can be induced into the captured CIRs if the channel under test (CUT) has a delay spread longer than the period of the $m$-sequence. For our PS sounder, the maximum distance ($d_m$) a ray can travel before starting to "wrap around" is approximated by $d_m \approx 2^{n-1}c/f_c = 87$ m [18], in which $n = 12$ is the shift register generator order and $c$ the speed of light. Importantly, due to the relaxed-rate sampling configuration of the PS sounder, the CUT should remain static for at least $T_{obs} = 19.9$ ms, which corresponds to a maximum Doppler frequency of $f_d = 50.2$ Hz and given by: $f_d = 2\nu \cos\theta \, f_{max}/c = 1/T_{obs}$, where $\theta$ is the angle of displacement, $\nu$ the speed of movement and $f_{max}$ the maximum transmitted frequency. Thus, in our case, the maximum $\nu$ of any object in the environment needs to be under 0.72 m/s, parameter that is more than maintained by avoiding any movement in the sounding area.

# 3 Description of Experiments

Two SISO LOS experiments are conducted to characterise UWB pulse-correlation distortion and errors in distance estimation. To this end, the equipment described in the previous section is used in an indoor office location and in an anechoic chamber.

## 3.1 Pulse-correlation distortion, experimental method

Limited resolution and intrinsic characteristics of measuring systems, and wireless transceivers in general, may induce distortion in test or data-carrying signals. To have an insight into this problem, measurements are conducted in a modern open-plan office in the central area of Bristol, UK. The sounded environment is populated with standard office scattering objects, but these are irrelevant for this work. The reason for this is that the measured CIRs are constrained to extract the unscattered LOS components only. In turn, this data is used to investigate the pulse-correlation distortion due to the inherent effects from the transmission-reception process.

The experiments thus consist of capturing sets of CIRs at different elevation angles and as a function of the distance between transmit and receive antennas. Of particular interest, changes in distance between antennas are chosen so that they are smaller than the spatial resolution of the PS

sounder ($s_r$). To this end, we define a fractional displacement $\Delta_d = 0.5$ cm, in which $\Delta_d < s_r/8$. The transmit ($tx$) and receive ($rx$) antennas are mounted on fibreglass masts at approximately $a_h = 1.3$ m from the floor or ceiling and initially distanced apart by $d_r = 1$ m. A total of nine ($L = 9$) locations are tested, with the distance for each location $l$ given by: $d_l = d_r + l\,\Delta_d$, where $l = 0, 1, ..., L-1$ and achieved by manually displacing the receive antenna mast over a pre-defined track. Consequently, $\{\forall\, l \;:\; l\,\Delta_d < s_r\}$. In addition, the transmit antenna mast is attached to the rotary part of an automated turntable, which allows the capture of CIRs at different elevation angles $\varphi_{tx}$ for each $l$.

Fig. 3 shows a diagram of the experiments, in which the transmit antenna is rotated[3] at a fixed location, while the receive antenna is displaced away from the transmit one. The figure also shows the coordinate system used with the biconical antennas, so that an azimuthal angle $\theta$, elevation angle $\varphi$ and distance $r$ define a parametric point of spatial radiation $P$. Note that, for these experiments, the Cartesian plane $(x, z)$ represents the horizontal plane.

Biconical antennas are known for having very similar radiation characteristics as a function of $\theta$ [19]. This was confirmed for our antennas by measuring three-dimensional radiation patterns in an anechoic chamber. Therefore, we concentrate on measuring $K = 180$ angular positions $\varphi_{tx}$ relative to a fixed $\varphi_{rx}$, so that $\varphi_{rx} = 0°$ and $\varphi_{tx} = -90°, -89°, ..., 89°$. For each measured point, denoted by $h_{l,k}$, a CIR is obtained as a result of averaging 512 measured CIRs, recorded in less than two seconds. This is possible because the environment was stable, as confirmed by previous equipment/environment stability and repeatability tests. As a result, we have a final set of 1,620 ($L \times K$) CIRs, resulting from a captured set of 829,440 CIRs.

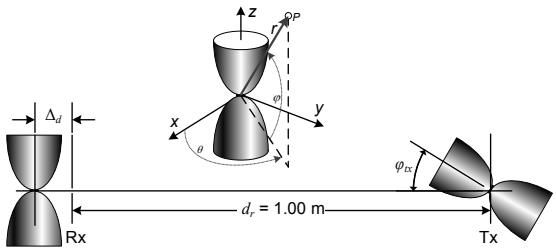


**Figure 3:** Top view of the pulse-correlation distortion experiments and the coordinate system used with the biconical antennas.

### 3.2 Distance estimation error, experimental method

Now, the turntable is replaced by an $(x, y)$ positioner, the SA is not used and measurements are taken in an anechoic chamber. Referring to the Cartesian coordinates for biconical antennas in Fig. 3, these experiments aim to determine the difference between the peak-estimated distance and the interpolated-estimated distance as a function of interpolation factor. This is, effectively, an approximation of the measured distance with different levels of accuracy.

The transmit and receive antennas are located inside an anechoic chamber, at approximately $a_h = 1.3$ m above the floor, and with equal polarization ($\varphi = 0°$). According to the antenna coordinates in Fig. 3, a change in the $(x, y)$ plane position represents a horizontal displacement.

In the chamber, the transmit antenna is kept at a fixed location in the far-field region of the receive antenna, whose mast is attached to the movable part of an $(x, y)$ servo positioner. Hence, the antennas have a minimum radial separation distance of around 5.8 m. The receive antenna is

[3]The antennas are physically mounted in such a way that they have the same polarization at $\varphi = 0°$ and rotation in the horizontal plane represents changes in the antennas' elevation angle.

automatically displaced in steps of 2 cm forming a horizontal grid of $30 \times 30$ cm. Accordingly, a set of 256 ($16 \times 16$) CIR measurements $h$ is taken by varying the $(x, y)$ position of the receive antenna relative to the transmit one. Note that for these experiments multipath components are greatly attenuated and external noise is significantly reduced. Nevertheless, each of the CIRs in $h$ is the result of averaging 256 captured CIRs.

A detailed description of a similar set-up is presented in [16], where the same approach was used to model the spatial and frequency dependent path loss of UWB signals when interacting with a small cylindrical scatterer.

# 4 Analytical Method and Results

An ideal pulse, represented by the Dirac delta function, would have infinite amplitude in time and infinite bandwidth in frequency [20]. In practice, pulse generation is subject to equipment accuracy, limited bandwidth and signal dispersion, between others [21]. Therefore, a pulse that is supposed to last for only one delay-sampling point is dispersed along several delay-sampling instances. This is a necessary evil since, otherwise, the detection of a perfect pulse would require a receiver with infinite accuracy or perfect synchronisation. In addition, as perfect synchronisation or UWB antennas with equal gain as a function of radiation angle are not physically feasible, some signal distortion is induced into the received signals, which may degrade the performance of communication systems even if there is no scattering interaction with the propagation environment.

Regarding the measured data, the CIRs from both experiments are the result of an up-converted baseband signal, whose system response has been removed by division after converting $h_{l,k}$ into the frequency domain ($H_{l,k}$) by using FFT [12]. This process creates a *removable discontinuity* [22] due to the signal's dc component being allocated at $f_c$ and then dividing it by a relatively small number. As the left- and right-hand limits of the signal component at $f_c$ exist, are convergent[4] and $f_c$ is always located at the same frequency-sampling point, its index, $f_c i$, is taken and the frequency components on its sides are averaged to replace the value it points: $H_{l,k}(f_c i) = \left[H_{l,k}(f_c i + 1) + H_{l,k}(f_c i - 1)\right]/2$. Having performed this correction, the CIRs are transformed back into the time domain and we can proceed to describe the methods to extract the unscattered LOS components from measurements, the post-processing of data and discuss the results for each experiment.

The data post-processing starts in a similar way for both experiments. We define an initial delay threshold index $i_{t1}$, which is based on the "time of flight" from transmit to receive antennas. A second threshold index $i_{t2} = i_{t1} + i_\delta$ is then defined to remove unwanted components from the received signal.

## 4.1 Pulse-correlation distortion due to angular and distance variations

To analyse the correlation distortion of unscattered LOS signals from the first experiment (Section 3.1), $i_\delta$ is estimated based on the delay that the first multipath component would have. Therefore, as we know that the antennas are at least $a_h = 1.3$ m from the floor and/or the ceiling, it can be easily shown that the minimum distance for the first multipath to travel between antennas is given by the $d_r/2$ point in the floor or ceiling, and that the distance this ray should travel is $d_m \geq \sqrt{d_r^2 + 4\,a_h^2}$ or more than 2.78 m. Since $d_r - d_m$ gives the additional distance to travel for this ray, we know that $\delta = c/(d_r - d_m)$. Considering the delay period of the sounder, the unscattered

[4] Considering $H_{l,k}$, we have that: $\lim_{f \to f_c^-} H_{l,k} \approx \lim_{f \to f_c^+} H_{l,k}$.

LOS components are thus the signals from the sample corresponding to $i_{t1}$ and up to $i_\delta = 41$ samples.

We now create a group of unscattered LOS pulses in which each pulse is given by $h_{l,k}(i_t)$, and where $i_t = i_{t1}, i_{t1}+1, ..., i_{t2}$. A replica of the original set is subsequently generated to create two groups: $T$ or pulse templates stored at the receiver and $R$ or received pulses. Having these sets, and after defining the CIRs' indices $\{\alpha, \gamma \in l\}$ and $\{\beta, \epsilon \in k\}$, the complex correlation ($\star$) between the different pulses $T_{\alpha,\beta}$ and $R_{\gamma,\epsilon}$ is estimated based on their covariance,

$$\mathrm{Cov}(T_{\alpha,\beta}, R_{\gamma,\epsilon}) = E\{T_{\alpha,\beta}\, R_{\gamma,\epsilon}\} - E\{T_{\alpha,\beta}\} \cdot E\{R_{\gamma,\epsilon}\},$$

so that:

$$T_{\alpha,\beta} \star R_{\gamma,\epsilon} = \frac{\mathrm{Cov}\left(\bar{T}_{\alpha,\beta}, R_{\gamma,\epsilon}\right)}{\sqrt{\mathrm{Cov}\left(\bar{T}_{\alpha,\beta}, \bar{T}_{\alpha,\beta}\right)\ \mathrm{Cov}\left(R_{\gamma,\epsilon}, R_{\gamma,\epsilon}\right)}}, \tag{1}$$

where $E\{\cdot\}$ is the expected value and $\bar{(\cdot)}$ the complex conjugate.

The analysis thus starts by estimating the complex correlation of pulses as a function of distance $l$ and angle $\varphi_{tx}$. Then, we average the angular results to obtain a single value per distance $l$. Note that the averaging of angular results per location $l$ is possible since the results are very similar.

Fig. 4 shows the orthographic projection of the correlation results as a function of distance shift. The initial distance between transmit and receive antennas is 1 m and it is represented by a 0 cm displacement in the plot. Analysis of results indicates that a correlation value of one may only be expected when correlating pulses with the same template. Otherwise, the correlation decreases gradually until reaching a correlation value of 0.4. It can also be noted that correlating against the next pulse does not always guarantee high correlation. This is clear when looking at the correlation values of the pulse measured at the initial position (0 cm) with the other pulses. In this case, the correlation increases as it is calculated with the pulses near to the next sampling point (4 cm).

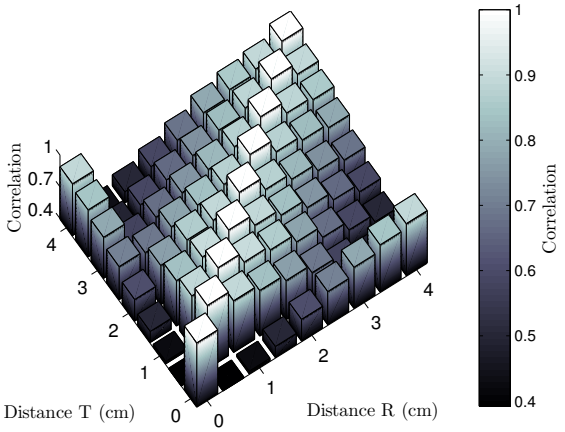


**Figure 4:** Correlation of received pulses as a function of distance and averaged over the angular elevation measurements. The initial distance between antennas is 1 m and, from this point, measurements are taken at 0.5 cm steps up to 4 cm. Correlation values vary between 0.4 and 1.

The correlation of received pulses as a function of radiation and/or capture angle is inherent to the characteristics of the antennas used. In this case, biconical antennas have very similar response as a function of azimuthal angle, but fluctuate as a function of elevation angle $\varphi$. Therefore, for our characterisation, it is sufficient to only measure the antenna response as a function of elevation

angle for one of its sides, or from 90° to −89°, in which 0° corresponds to the transmit and receive antennas facing each other with the same elevation angle. Complex correlation is now calculated as a function of elevation angle for each of the $l\,\Delta_d$ points. The results from the $L$ locations are then averaged to obtain a single set of values as a function of elevation angle $\varphi_{tx}$.

Fig. 5 shows the orthographic projection of the correlation results as a function of elevation angle. Results in the figure are constrained from 80° to −80° as the unscattered LOS signals after these angles have less than 20 dB amplitude compared to the one at $\varphi_{tx} = 0°$. Results from the correlation calculations show that only pulses radiated from the same angle have a correlation value of one and differences of approximately ±5° still offer high correlation. It is also noted that corresponding negative and positive elevation angles have strong correlation and that the minimum expected correlation is 0.5.

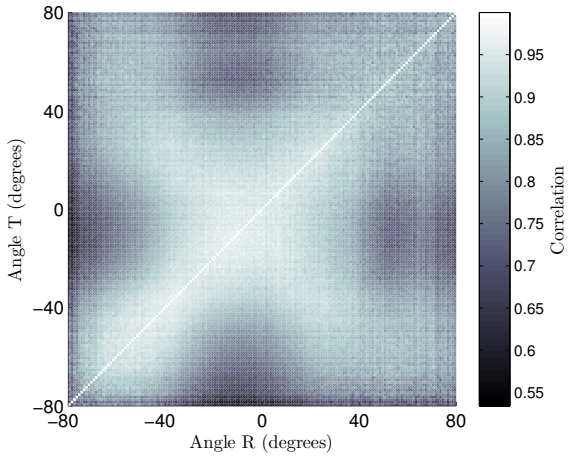


**Figure 5:** Correlation of received pulses as a function of elevation angle between transmit and receive antennas and averaged over the different transmit and receive 0.5 cm antenna separations. Correlation values vary between 0.5 and 1.

Now only the pulses radiated and captured at zero degrees elevation are analysed for the different measured points in distance. These pulses are then normalised to the pulse with the strongest peak power, FFT interpolated [13], and realigned to have their peak value at the same sampling point. As a sanity check, the complex FFT interpolation technique was compared against the *spline* interpolation of the real and imaginary components of the complex pulses, [23]. Results from this analysis indicate that the two techniques produce very similar interpolation results for the input signals. Therefore, only the FFT interpolation technique is used for interpolating the measured pulses.

Fig. 6 shows the unscattered LOS pulse templates obtained at different linear locations and zero degree elevation angle. Note that correcting the real distance for each pulse is not possible due to sampling limitations, but have been normalised to the power of the strongest signal from the measurements. Normalising the captured pulses to their respective peak power would induce a wrong comparison because the *true peak power* of each pulse is unknown as a consequence of sampling limitations. In Fig. 7 the same pulse templates are FFT interpolated, realigned in time, normalised to the set maximum power and shifted in time so the peaks happen at the same sampling instant. The time shifting of the interpolated pulse templates is possibles as the time resolution has been increased and a more accurate peak power has been estimated.

The measured set of pulses, at zero degree elevation, was intentionally chosen for analysis to

have an insight into why the response of the biconical antennas we use, at this particular elevation angle, presents decreased energy at around 7 GHz [24]. After interpolation, it is clear that the pulses measured at this elevation angle present a strong secondary reflection, which causes a destructive effect around the 7 GHz frequency region.

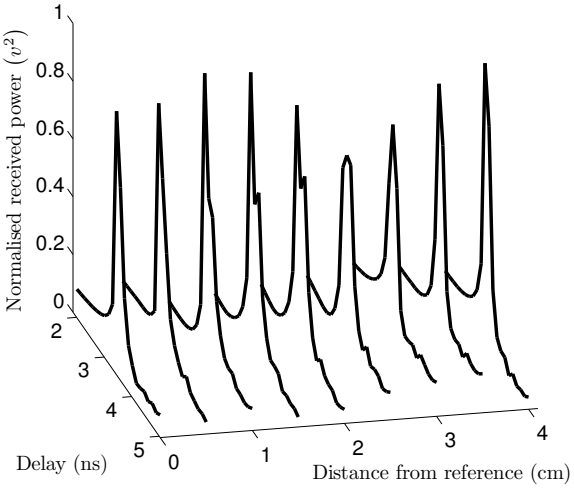


**Figure 6:** Measured unscattered pulses at different $l$ distances.

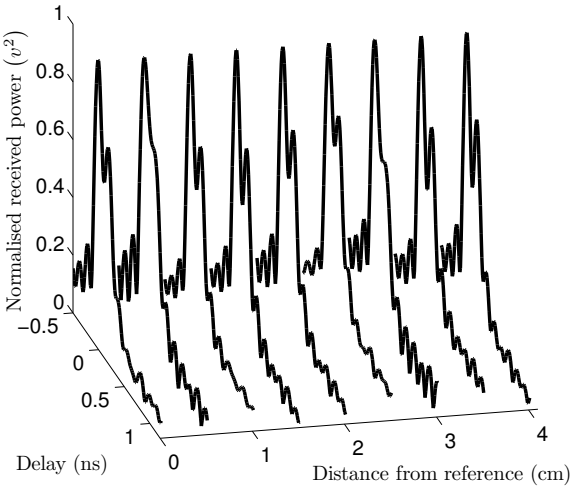


**Figure 7:** FFT-interpolated unscattered pulses at different $l$ distances.

The oscillatory behaviour of the FFT-interpolated pulses, in Fig. 7, is due in part to the use of a rectangular window in the interpolation process. This effect is also due to the oscillatory behaviour of the real and imaginary components of the original pulses. These fluctuation greatly disappear when the pulses are sampled at the rate of the original measurements as the sampled points correspond to equally spaced points on a constant oscillation process. This effect can be appreciated from the noise floor of the measured pulses in Fig. 6.

The complex correlation is now estimated for the two sets of pulse templates. The results from the calculations are presented in orthographic projections for the measured pulses (Fig. 8) and the FFT-interpolated pulses (Fig. 9) as a function of distance shift and starting from a 1 m reference point or 0 cm distance in the plot.

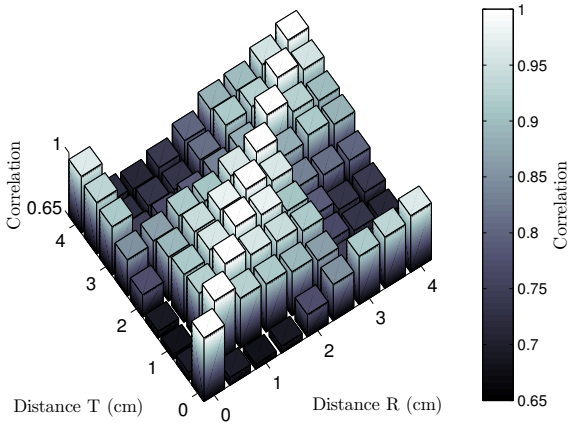


**Figure 8:** Correlation of measured pulses. Correlation values vary between 0.65 and 1.

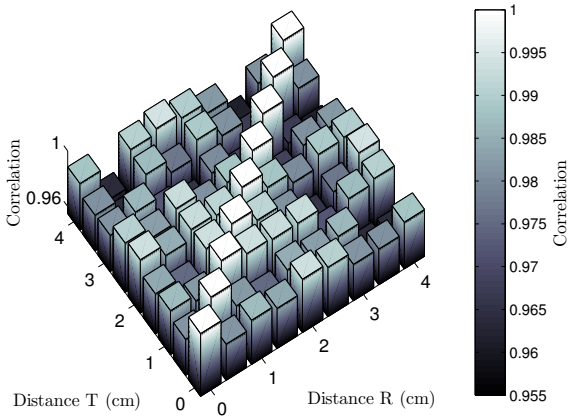


**Figure 9:** Correlation of FFT interpolated pulses. Correlation values vary between 0.96 and 1.

Analysis of results from the measured pulses indicates that the correlation values fluctuate from 0.65 to 1. The range in correlation is certainly better than when more angular variations are included (0.4 to 1 in Fig. 4). In the case of the FFT-interpolated pulses, the correlation ranges between 0.96 and 1. This proves that the FFT interpolation of different pulse templates from the same combination of radiation and capture angles, from transmit and receive antennas, produce highly correlated templates. This result can be used to increase the accuracy of the deconvolution process by using an FFT-interpolated pulse template to generate several pulse templates and maximise the correlation between a received measured pulse and a known pulse template.

Considering the complexity of adding several pulse templates to extract information from measured CIRs, the correlation response of the antennas as a function of angle is constrained to remove negative elevation angles. In this particular case, the reduction on the number of pulse templates used for deconvolution is possible as the radiation characteristics of the antennas are known.

## 4.2 Error in distance estimation due to sampling resolution

From the experiments in Section 3.2, the estimation of distance between two antennas may be referred to the distance travelled by a pulse from the transmit to the receive antenna. However,

due to practical limitations, the receiver cannot detect the signal with infinite accuracy and only samples of it are recorded. The problem with this limitation is that a pulse may last for more than one sampling instant and its true peak may lie between samples. The lack of more sampling resolution makes the receiver to get the time of flight of the strongest received signal and estimate the distance between transmit and receive antennas based on it.

For this test and considering the results in the previous section, the 256 recorded CIRs are FFT interpolated with different interpolation factors $I_f$, which range from: no-interpolation ($I_f = 1$) to the CIR being ten times its original size ($I_f = 10$). The distance error, $D_e$, is calculated per CIR by measuring the time of arrival of the peak power, extracted from the power-delay profile (PDP) of the interpolated CIR, and calculating the distance shift ($d_s$) relative to the nearest sampling point $d_r$. distance errors from $I_f = 1, 2, ..., 9$ are measured against $I_f = 10$:

$$D_e(I_f) = d_r \left| \frac{d_s(I_f = 10)}{10} - \frac{d_s(I_f)}{I_f} \right|, \tag{2}$$

in which $|\cdot|$ is the absolute value. Note that $d_s$ from the highest interpolation order ($I_f = 10$) is used as reference to compare $d_s$ estimates from other $I_f$ values.

The $D_e$ results are then statistically analysed to find their normal distribution parameters or mean $\bar{D}_e$ and variance $\sigma^2$. These values, along with the maximum (max.) and minimum (min.) errors, are summarised in Table 1. These values can be used to have an idea of the expected distance error estimation when interpolation or received pulses is available.

**Table 1:** Normal Fitting Parameters for Distance Estimation Error in cm*.

| $I_f$ | $\bar{D}_e$ | $\sigma^2$ | max. | min. |
|---|---|---|---|---|
| 1 | 3.99 | 1.37 | 6.46 | 2.15 |
| 2 | 1.91 | 0.60 | 3.02 | 0.86 |
| 3 | 1.04 | 0.21 | 1.87 | 0.14 |
| 4 | 0.63 | 0.07 | 1.29 | 0.0 |
| 5 | 0.41 | 0.07 | 0.86 | 0.0 |
| 6 | 0.33 | 0.03 | 0.86 | 0.0 |
| 7 | 0.25 | 0.03 | 0.62 | 0.0 |
| 8 | 0.21 | 0.02 | 0.54 | 0.0 |
| 9 | 0.16 | 0.01 | 0.48 | 0.0 |

* Approximated to nearest fraction.

Using the fitting values from Table 1 and the evaluation of 2, Fig. 10 shows the $D_e$ cumulative density function (CDF) for different $I_f$ and their normal fittings. Note that the rightmost curve, $I_f = 1$, is the non-interpolated case. From the plot, because the received pulses span over three samples ($P_s = 3$), the maximum $D_e$ is $\pm d_r\, P_s/2$. This can be appreciated from the results in the figure when no interpolation is used ($I_f = 1$).

## 5 Conclusions

Ultrawideband (UWB) measurements were used to prove the effects of correlating captured pulses at the receiver with pulse templates that may differ from received *unscattered* signals. We thus found that: (i) Correlation values varied from full correlation to 40% if the pulses differed as a result

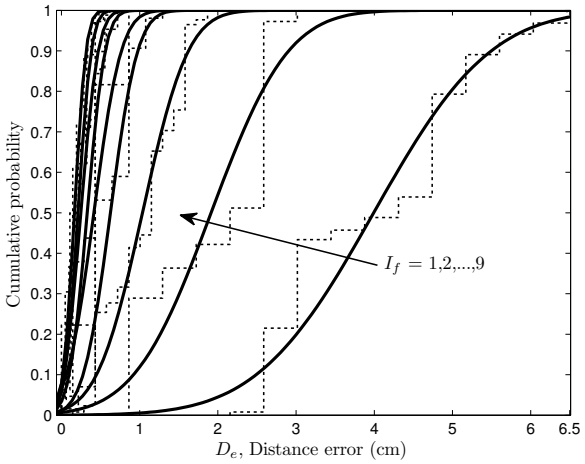


**Figure 10:** CDF and normal distribution fitting of distance error.

of distance changes, between transmit and receive antennas, smaller than the spatial resolution of the transceivers. (ii) When the distance was maintained and the angle of departure/arrival changed between antennas, correlation values changed from full correlation to 50%. (iii) While the radiation patterns of transmit and received antennas remained aligned and sub-spatial-resolution movements were induced, pulse correlation changed from full to 65%. However, if interpolation of these pulses, using the fast Fourirer transform (FFT), is done to derive templates, then the minimum correlation value increases to 96%.

Hence, if correlation of pulses is required for extracting the energy from channel impulse responses (CIRs), multiple templates need to be used and considered as a function of angle of radiation/capture and distance displacement in fractions of the transceivers' spatial resolution. Otherwise misleading results are expected. This observation can also help to improve the location awareness of ultrawideband (UWB) systems as, if multiple pulses can be discerned, direction of departure/arrival can be used to increase distance estimation values.

Having proved the advantages of using the FFT interpolation method in this case, error in distance estimation was measured for different interpolating values. As a result, the error estimation was shown to follow a normal distribution and fitting curves were presented with their corresponding parameters.

It is left as a subject of future research the deployment of iterative algorithms, such as CLEAN, with adaptive pulse templates as result of the findings presented in this paper.

## Acknowledgements

The authors gratefully acknowledge the directors of Toshiba Research Europe Limited, Telecommunications Research Laboratory, for their support and permission to publish this work.

## References

[1] A. Phan, R. Farrell, M.-S. Kang, S.-K. Han, and S.-G. Lee, "Low-power sliding correlation cmos uwb pulsed radar receiver for motion detection," in *Circuits and Systems, 2009. ISCAS 2009. IEEE International Symposium on*, may 2009, pp. 1541 –1544.

[2] F. Zhang, R. Gharpurey, and P. Kinget, in *Radio Frequency Integrated Circuits Symposium, 2008. RFIC 2008. IEEE*, 17 2008-april 17, pp. 31 –34.

[3] R. Cardinali, L. De Nardis, M.-G. Di Benedetto, and P. Lombardo, "Uwb ranging accuracy in high- and low-data-rate applications," *Microwave Theory and Techniques, IEEE Transactions on*, vol. 54, no. 4, pp. 1865 –1875, june 2006.

[4] M. Skolnik, *Introduction to Radar Systems*, 3rd ed. New York: McGraw-Hill, 2000.

[5] N. Neretti, N. Intrator, and L. Cooper, "Adaptive pulse optimization for improved sonar range accuracy," *Signal Processing Letters, IEEE*, vol. 11, no. 4, pp. 409 – 412, april 2004.

[6] G. Immaculate Mary and V. Prithiviraj, "Test measurements of improved uwb localization technique for precision automobile parking," in *Recent Advances in Microwave Theory and Applications, 2008. MICROWAVE 2008. International Conference on*, nov. 2008, pp. 550 – 553.

[7] E. Pancera and W. Wiesbeck, "Correlation properties of the pulse transmitted by uwb antennas," in *Electromagnetics in Advanced Applications, 2009. ICEAA '09. International Conference on*, sept. 2009, pp. 701 –704.

[8] K. Witrisal and M. Pausini, "Statistical analysis of uwb channel correlation functions," *Vehicular Technology, IEEE Transactions on*, vol. 57, no. 3, pp. 1359 –1373, may 2008.

[9] A. Muqaibel, A. Safaai-Jazi, B. Woerner, and S. Riad, "UWB channel impulse response characterization using deconvolution techniques," in *Circuits and Systems, 2002. MWSCAS-2002. The 2002 45th Midwest Symposium on*, vol. 3, Aug. 2002, pp. III–605–8 vol.3.

[10] J. A. Högbom, "Aperture synthesis with a non-regular distribution of interferometer baselines," *Astronomy and Astrophysics Supplement, Vol. 15, p.417 (A&AS Homepage)*, June 1974.

[11] R. Vaughan and N. Scott, "Super-resolution of pulsed multipath channels for delay spread characterization," *Communications, IEEE Transactions on*, vol. 47, no. 3, pp. 343–347, Mar 1999.

[12] R. Cepeda, S. C. J. Parker, and M. Beach, "The measurement of frequency dependent path loss in residential LOS environments using time domain UWB channel sounding," in *Ultra-Wideband, 2007. ICUWB 2007. IEEE International Conference on*, 24-26 Sept. 2007, pp. 328–333.

[13] W. G. Hawkins, "FFT interpolation for arbitrary factors: a comparison to cubicspline interpolation and linear interpolation," in *Nuclear Science Symposium and Medical Imaging Conference, 1994., 1994 IEEE Conference Record*, vol. 3, Norfolk, VA, USA, Oct. 30–Nov. 5, 1994, pp. 1433–1437.

[14] J. Sachs, R. Herrmann, M. Kmec, M. Helbig, and K. Schilling, "Recent advances and applications of m-sequence based ultra-wideband sensors," in *Ultra-Wideband, 2007. ICUWB 2007. IEEE International Conference on*, 24-26 Sept. 2007, pp. 50–55.

[15] IRK Dresden, (2009, April). [Online]. Available: http://www.irk-dresden.de/en/

[16] R. Cepeda, W. Thompson, and M. Beach, "On the mathematical modelling and spatial distribution of UWB frequency dependency," in *Wideband and Ultrawideband Systems and Technologies: Evaluating current Research and Development, 2008 IET Seminar on*, Nov. 2008, pp. 1–5.

[17] *402/403/404XE Series Product Manual*, Parker Hannifin Corp. September 2006 (2009, August). [Online]. Available: http://www.compumotor.com/manuals/XE/xeprodmanrev2.pdf

[18] J. Sachs, P. Peyerl, P. Rauschenbach, F. Tkac, M. Kmec, and S. Crabbe, "Integrated digital UWB-Radar," in *Ultra-Wideband Short-Pulse Electromagnetics 6*. 255-259, E. L. Mokole, M. Kragalott, and K. Gerlach, Eds. Kluwer Academic / Plenum Publishers, 2003.

[19] C. A. Balanis, *Antenna Theory - Analysis and Design*, 2nd ed. John Wiley & Sons, 1997.

[20] J. Proakis, D. Manolakis, D. Manolakis, and J. Proakis, *Digital signal processing: Principles, algorithms, and applications*. Prentice Hall New Jersey, 1996.

[21] J. Andrews, "UWB signal sources, antennas & propagation," August 2003.

[22] S. Malik and S. Arora, *Mathematical analysis*. New Age International, 1992.

[23] C. de Boor, *A Practical Guide to Splines*. Springer, 1978.

[24] R. Cepeda, W. Thompson, M. Beach, and J. McGeehan, "On the measurement and simulations of the frequency dependent path loss and MB-OFDM," in *Ultra-Wideband, 2009. ICUWB 2009. IEEE International Conference on*, Vancouver, BC, Sep. 9–11, 2009, pp. 321–325.